Combinatorial fake discriminatory selections for combined dE/dx and disappearing track search with the ATLAS detector

by

AIDAN GARDNER-O'KEARNY

A THESIS

Presented to the Department of Physics and Robert D. Clark Honors College in partial fufillment of the requirements for the degree of Bachelor of Science

May 2025

An Abstract of the Thesis of

Aidan Gardner-O'Kearny for the degree of Bachelor of Science in the Department of Physics, to be taken May 2025

Approved:

Primary Thesis Advisor

The Standard Model of particle physics is a highly accurate physical theory, one of the most successful we have conceieved. Despite its high precision, there are a number of areas in which the Standard Model fails to provide satisfactory answers. To search for long-lived, massive particles as part of a supersymettric extension to the Standard Model, we are using an analysis strategy based around a disappearing track and anomalous ionization energy signature. A major background for this search are combinatorial fakes, which have proven to be difficult to select against. This thesis examines the composition and behavior of this background, and searches for additional selections that would better discriminate against background in favor of signal.

Acknowledgements

I would not be here without many, many wonderful people who have helped guide and support me during my time at UO. I'd like to start by thanking my parents, who encouraged this instead of suggesting I study something with practical applications, this is a lot more fun than having a real job.

Graduate student Nathan Young had the daunting task of helping someone who bricked their computer trying to install ROOT make useful contributions to an analysis, and has never once complained about the large number of things we ask him to do.

Owen Mitchem, Christina Dorofeev, Elise Jaremko, Isabelle Dana, Katie Linnenkohl, you all are living proof that half the fun of doing something difficult is getting to complain about how difficult it is with good friends, thank you.

Many thanks to Gantt Gurley for being so willing to assist in this process and for his constant enthusiasam.

And of course, the most massive of thank yous to my advisor, Laura Jeanty. It is safe to say that I owe essentially all of my success to your mentorship and guidance. You gave me the freedom to make naive mistakes and used them as teaching moments before turning me in the right direction. Thank you for taking a chance on me.

Contents

List of Figures

1 Introduction

1.1 The Standard Model

The Standard Model (SM) of particle physics is one of the most successful physical theories that we have ever conceived. Utilizing 17 fundamental particles and analytical descriptions of their interactions, it describes all of the ordinary matter in the universe as well as three of the four fundamental interactions. Particles in the Standard Model fall into one of two categories, based on their spin. Fermions, particles with half-integer spin, are matter particles and can be further divided into two families; leptons and quarks. Fermions come in three generations, each with identical quantum numbers but increasing mass. Gauge bosons (integer spin particles) are the force carriers of the Standard Model, allowing momentum and energy to be transferred between particles. The Higgs Boson, discovered in 2012, is a scalar particle that gives other particles their mass [7].

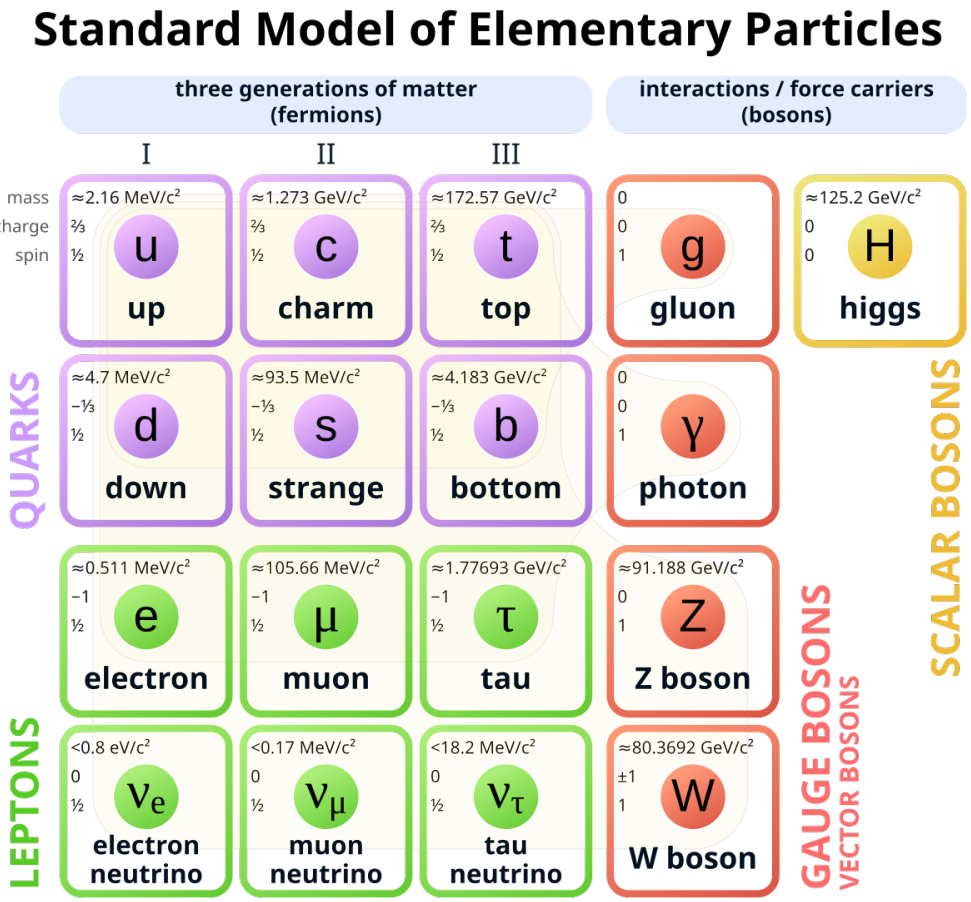

Figure 1: The Standard Model. Source: Wikipedia, "Standard Model"

The Standard Model is an amalgamation of several different quantum field theories, each describing different forces. These theories provide us a quantutitative method to calculate parameters that can be measured experimentally. The accuracy of these predictions is extremely high, with some of the most impressive predictions agreeing with experiment out to twelve decimal places, such as the electron's anomalous

magnetic dipole moment [8]. These predictions can be calculated using Feynmann diagrams, representations of potential methods by which a given process could happen. A generic Feynmann diagram is shown in Fig 2.

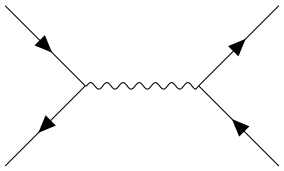

Figure 2: A generic Feynman diagram showing a fermion and an anti-fermion interacting to form another fermion anti-fermion pair.

Each vertex in a Feynmann diagram contributes a factor of α_i to a predicted quantity, where α_i is the coupling constant associated with the interaction governing that vertex. These coupling constants are not, in fact, constant, but instead run with the momentum of the particles involved. Despite this, coupling constants are oftentimes small, and each additional factor usually decreases the probability amplitude of a given diagram. In this way, increasingly complicated methods of a process occurring tend to be naturally suppressed.

1.2 Motivation For Beyond Standard Model Physics

Despite its incredible accuracy, there are several areas in which the Standard Model is lacking. For instance, the hierarchy problem (where we question why the measured Higgs mass is 125 GeV rather than on the order of the Planck mass) is something for which the Standard Model is unable to provide a satisfactory answer. Additionally, the coupling constants do not converge in the Standard Model, despite it being a natural prediction for them to (see Fig 3).

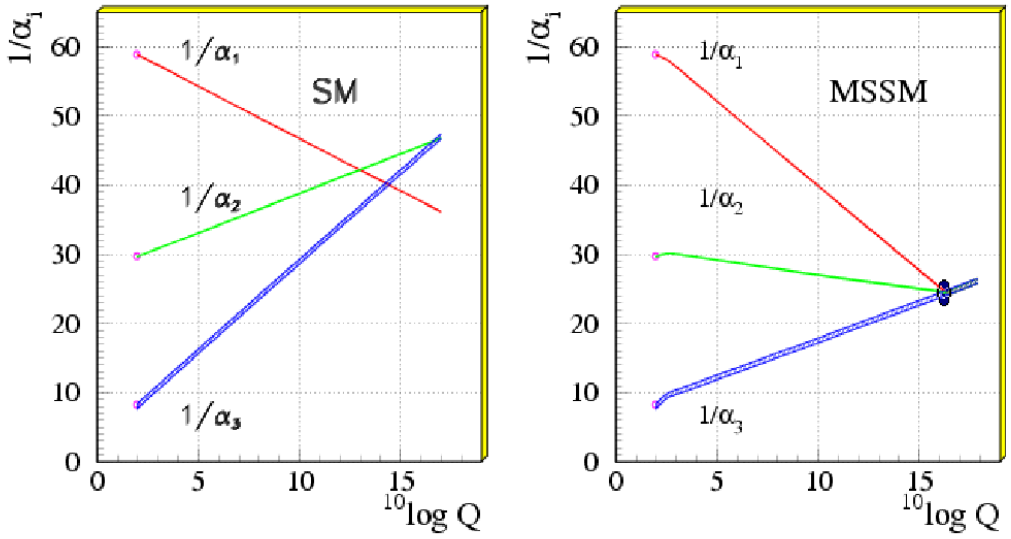

Figure 3: Coupling constants in both the Standard Model and in Supersymmetry. Under the SM they do not unify, whereas under SUSY they do [1].

Possibly the most compelling motivations for new physics is dark matter. Numerous experimental lines of evidence suggest that there is more matter in the universe than can be seen, implying that there exists a form of matter that is massive, stable on cosmological scales, and electrically neutral. The only Standard Model particle that fits this description are the neutrinos (ν_ℓ), but due to current constraints on neutrino masses ($\sum m_\nu = 0.12$ eV [9]), current estimates place them on $\mathcal{O}(0.01)$ of all dark matter [10]. The rest of the observed dark matter has no Standard Model candidate that could compose it, providing strong evidence for the existence of new physics beyond the Standard Model.

Because of these issues, there is strong motivation for extensions to the Standard Model, aimed at resolving one or more open problem. There are many such extensions, from hidden valley models that provide very natural dark matter candidates [11], to additional Higgs sector models that address CP violation in the Higgs sector [12]. This work will focus on a search for one of the most bold and histoically popular Beyond Standard Model theories, Supersymmtery.

1.3 Supersymmetry

Motivated by resolving the hierarchy problem, Supersymmetry (SUSY) introduces a superpartner for every Standard Model particle, with that superpartner having a spin differing by $\frac{1}{2}$ [13]. This has the effect of making all SM fermions have bosonic superpartners and all SM bosons having fermionic superpartners. This addition creates new Feynmann diagrams that suppress the processes that would result in a high Higgs mass in the Standard Model, providing an answer as to why the Higgs mass is 125 GeV.

This theoretical framework would have many additional consequences beyond solving the hierarchy problem. It would provide a unficiation of the fundamental forces (see Fig 3) as well as providing an excellent dark matter candidate. The lightest super-symmetric particle is predicted to both be stable and neutral and could be created with the correct relative abundance to match the amount of dark matter that is observed [14].

We are interested in a model of SUSY in which the lightest super-symmetric particle is the neutralino $(\tilde{\chi}^0)$. Some of these models come with interesting experimental signatures. Two example production channels from a pp collision are shown in Fig 4.

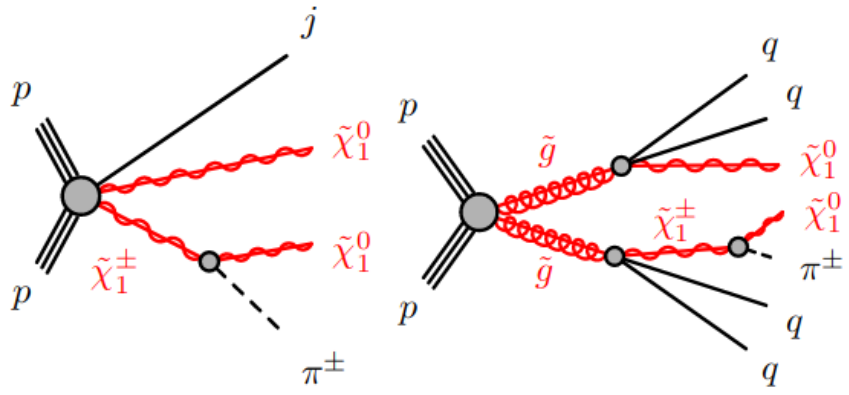

Figure 4: Electroweak and strong production channels of a $\tilde{\chi}^\pm$. Particles in the final state include soft pions and $\tilde{\chi}^0$, a potential dark matter candidate. (N. Young).

These production processes allow us to search for the neutralino. As the neutralino is a neutral and stable

particle, it would be difficult, if not impossible, to detect using standard techniques. Instead, we will be able to search for the neutralino by searching for the intermediate states of this process. These particles (our analysis searches for charginos ($\tilde{\chi}^{\pm}$) and staus ($\tilde{\tau}^{\pm}$)) would be charged and potentially long-lived, guiding the search strategy described in Section 2.3.

1.4 Long-Lived Particles

Particle lifetime arises from a number of different properties. A particle's lifetime is given by [15]

$$\tau^{-1} = \Gamma = \frac{1}{2m_x} \int d\Pi_f |\mathcal{M}(m_x \to \{p_f\}|^2$$

where $\mathcal{M}$ is the matrix element of the particle decaying to its final states.

This calculation often ends up being complicated, and while it can be used to calculate the lifetime of any particle, there are three general rules for predicting whether a particle will be long-lived:

1. The final products after a decay occurs have near the same mass as the original particle. This means there isn't much leftover energy to make the decay happen. This applies to the neutron, where β-decay is the process $n \to p + e^- + \bar{\nu}$. The mass of the proton is similar to that of the neutron (938.3 MeV to 939.6 MeV), so the neutron has a fairly high lifetime of 885.7 seconds.

2. The coupling involved is small. The stronger the interaction and the coupling to that interaction, the more likely the decay is to happen, so smaller couplings leads to longer lifetimes. This can be seen in the case of the Δ^- decay. Similar to the Σ^- the Δ^- is a baryon with a -1 charge. However their lifetimes are very different with the Δ^- having a lifetime of 5.6×10^{-10} seconds and the Σ^- having a lifetime of 1.48×10^{-24} seconds. This is due to the Δ^-'s decay being mediated through the strong force and the Σ^-'s decay being mediated by the weak force. The strong force has much larger coupling than the weak force so decays it mediates happen much quicker, leading to the Σ^-'s longer lifetime.

3. If a virtual particle involved in the decay is very off-shell, then the particle is less likely to decay, as that requires more energy to be borrowed in order for the process to occur. This applies to the decay of pions. Charged pions ($\pi^{\pm}$) decay weakly via a W boson, versus neutral pions (π^0) decay via QED processes. The W boson is much heavier than the pion and so is very off shell, the neutral pion's decay is mediated by a quark, which is lower mass than a pion. The lifetime of the charged pion is thus much higher at 2.6×10^{-8} seconds than the neutral pion's lifetime of 8.4×10^{-17} seconds.

The chargino could be long-lived due to its final states being nearly the same as its initial mass. From Figure 4 we can see that the decay products of a chargino are a neutralino and a charged pion. In a specific model of Supersymmetry, the difference in mass of the chargino and neutralino has been calculated to be $\mathcal{O}(100$ MeV) [5] and the mass of the pion is 135 MeV. This leads to the chargino having a lifetime of order 0.1 ns.

2 The Dissappearing Track and dE/dx Analysis

2.1 The LHC

Located at the border of Switzerland and France near Lake Geneva, the Large Hadron Collider (LHC) is a circular particle accelerator that represents the apex of modern experimental physics. After beginning operation in 2008, the accelerator has achieved a center of mass energy of $\sqrt{s} = 13.6$ TeV and is the most powerful accelerator operating currently.

The LHC accelerates bunches of protons up to $\beta > 0.9999$ by the use of 8.3 T electromagnets and then colliding them. Protons are grouped in bunches of 10^{11} with 2800 bunches in the detector at any given time. Bunches are collided every 25ns [16]. This correlated to 26 fb^{-1} of data during run 1 and 147 fb^{-1} of data during run 2. The LHC is currently in its third run and will aim to produce 250 fb^{-1} of data by its end date in 2025 before going into another period of long shutdown for repairs and upgrades [3].

The LHC has many experiments opperating on it, collectively forming the largest international collaboration of physicists in the world. Among these are ALICE, LHCb, FASER, CMS and ATLAS. This thesis concerns an analysis being conducted by the ATLAS Experiment.

2.2 The ATLAS Detector

Pictured in Fig 5, the ATLAS detector is a general purpose detector, covering nearly 4π of solid angle around the interaction spot.[1] Best known for its discovery of the Higgs boson in 2012 [17], it is on the forefront of the experimental effort to search for new Beyond Standard Model physics.

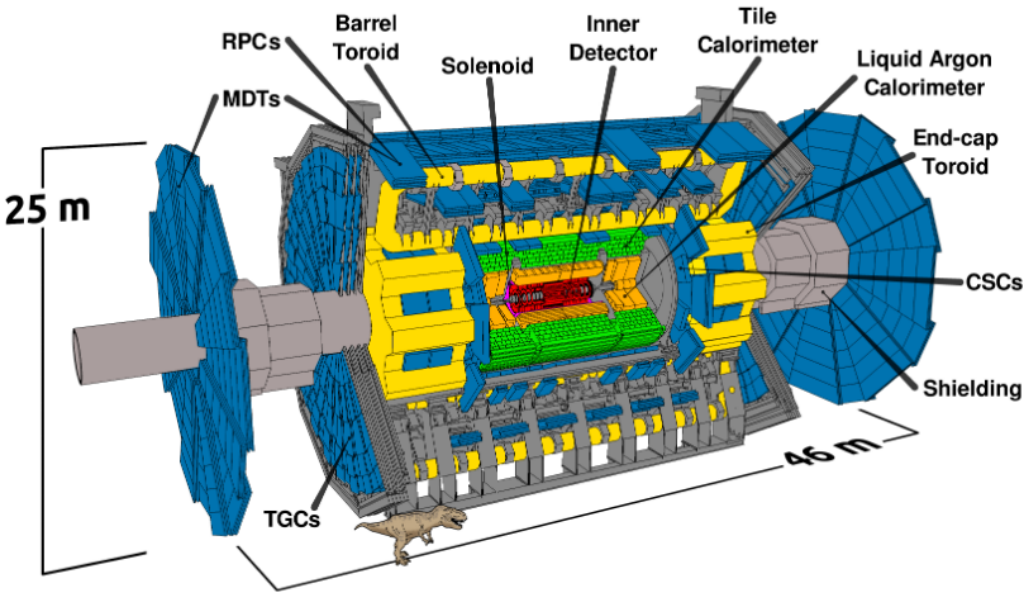

Figure 5: The ATLAS Detector, with a T-Rex for scale [2].

The detector is composed like an onion, with different layers built radially around the beampipe. There is the inner detector, meant for reconstructing charged particle trajectories, the electromagnetic calorimeter,

[1] ATLAS uses a right handed coordinate system (z, η, ϕ), where angular distance is defined in units of $\Delta R = \sqrt{\Delta\eta^2 + \Delta\phi^2}$. η is the pseudorapidity of a particle $\ln\left(\cot\frac{\theta}{2}\right)$, and is a Lorentz-invariant quantity.

meant for recording the energy of particles that interact electromagnetically, the hadronic calorimeter, meant to reconstruct hadronic particles that make it through the first two layers, and the muon spectrometer, which reconstruct muons, which live long enough to pass through the other layers.

Of special interest to the disappearing track and dE/dx analysis is the Inner Detector, shown in Fig 6. The inner detector is made up of three distinct subsystems, the Pixel Detector, the SCT layers, and the TRT. The Pixel Detector is made up of four layers (the IBL located at 33.25 mm from the beamline and three additional pixel layers going out to 122.5 mm from the beamline) made up of a mesh of individual pixels that are capable of recording the direction and charge deposited by a particle passing through it. This charge and direction can be converted to a measurement of the ionization energy loss, or dE/dx.

The SCT's first layer is located 299 mm from the beamline, which is farther than the target decay distance for our model of interest. As such, we veto any tracklets with hits in the SCT.

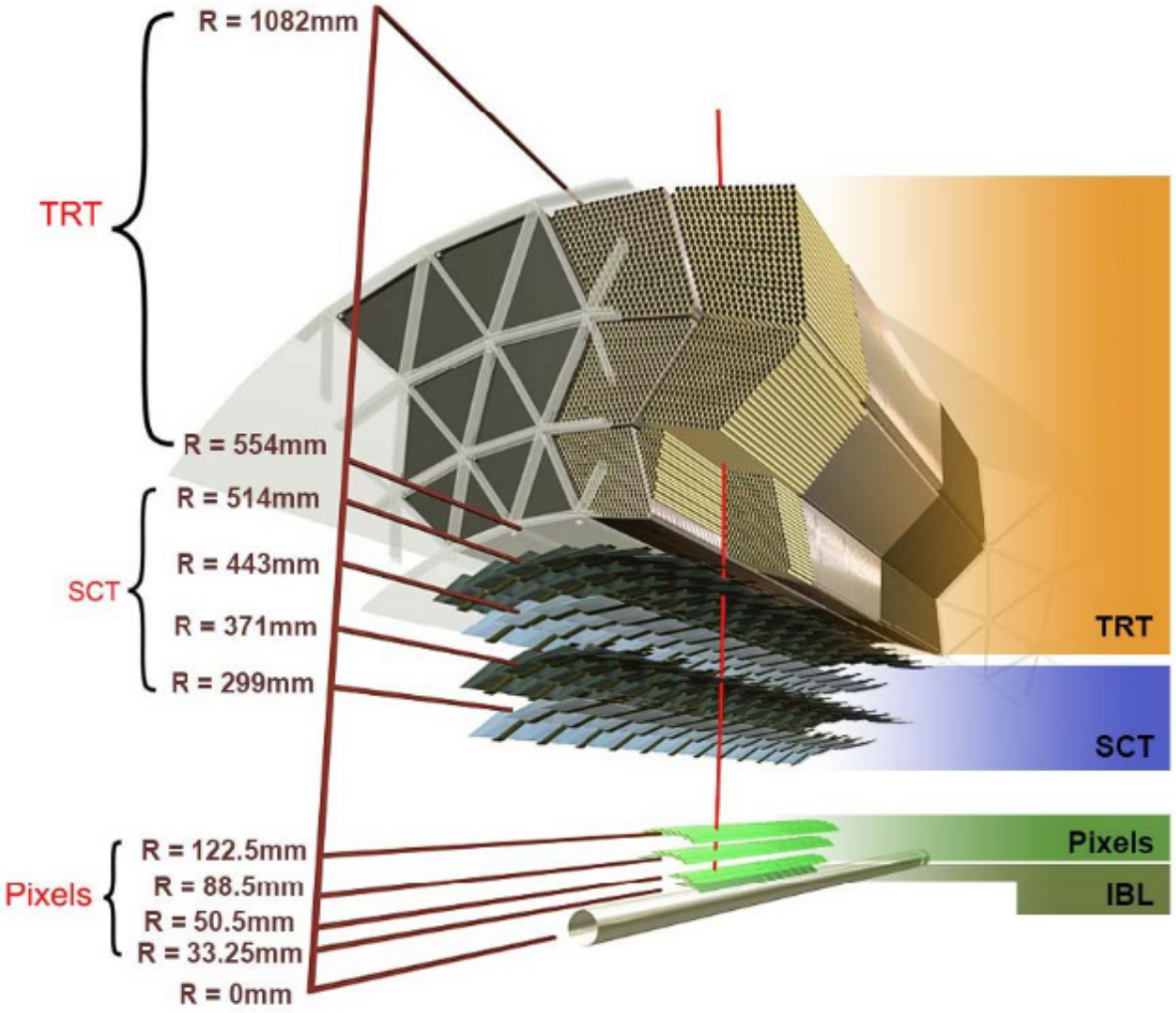

Figure 6: The ATLAS Inner Detector [3].

Due to the large number of pp interactions and the composite nature of protons, not every single collision within the ATLAS detector is of interest to us, and there must be many more collisions than could be recorded. This means that there must be some selection of which data to record. This is accomplished

with the ATLAS Trigger and Data Aquisition System (TDAQ) [3]. The trigger system operates in two components, the Level-1 Trigger (L1) and High-Level Trigger (HLT). The L1 system operates at a high speed and is used to make quick decisions about which events to throw out and which events to pass on to the HLT based on energy deposited in the calorimeters and muon spectrometer. The HLT operates at a slower speed, and as such can use more precise information to make decisions. Combined, the TDAQ reduces the amount of incoming information down to a more managable 3 kHz.

2.2.1 Clusters

It is worth making special note of how a particle traversing the inner detector is turned into a track or tracklet, and how track level measurements arise. The pixel layers are composed of a number of individual silicon pixels. As a charged particle passes through a pixel, it frees electrons within the pixel. Pixels that have enough electrons freed for a long enough period of time can be grouped together into objects called clusters (Fig 7). Clusters in different layers are then grouped together into tracks by a track reconstruction algorithm. A track is a representation of the path a particle takes through the detector, short tracks are known as tracklets, and are defined as having seven or less hits. Tracks can be parametrized in the form

$$d_0, z_0, \phi, \theta, \frac{q}{p}$$

where d_0 and z_0 are the transverse and longitudinal impact parameters, ϕ is the angle of rotation around the beamline, θ is the polar angle from the beamline, and $\frac{q}{p}$ is the ratio of the particle's charge to its momentum [2]. Once a track is defined its ionization behavior can be calculated.

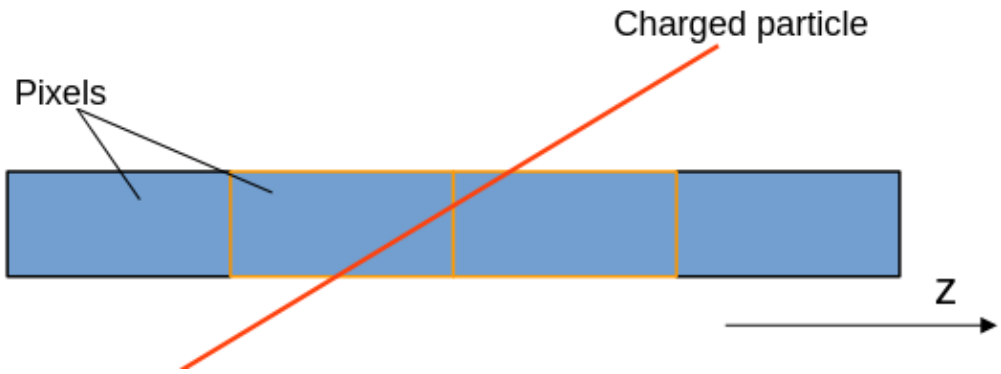

Figure 7: A cartoon of how a particle passing through a pixel layer forms a cluster by exciting several individual pixels. [4]

2.3 The Analysis

One of the most exciting new analyses happening with ATLAS is the dE/dx and Disappearing Track search. This search looks for heavy, charged particles utilizing a disappearing track and ionization energy based signature. ATLAS has performed analyses based around both of these signatures individually using the Run 2 data [5][18]. The CMS experiment performed an analysis based on this combination of signatures

[19], however we expect to gain sensetivity in the pure Wino case. Current limits from the disappearing track search place lower limits on the Wino mass of 850 GeV (see Fig 8).

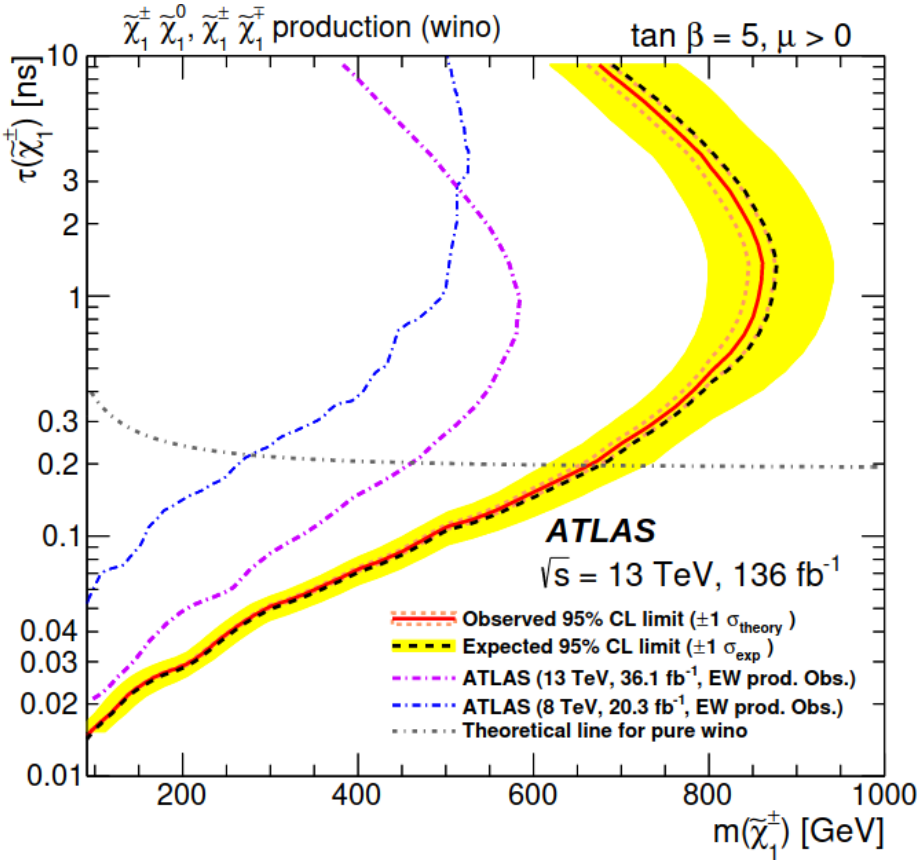

Figure 8: Exclusion limits from disappearing track search [5].

The dE/dx signature utilizes the ionization energy loss of a particle behind as it passes through the detector as a discriminant between signal and background. Cluster dE/dx is calculated as the average ionization energy per path length. As a particle passes through a pixel in the pixel layer, it frees some number of electrons, and this ionization can be converted into an energy which can be normalized by the path the partile took through the pixel. The collected dE/dx values for each hit in a track are then averaged using a truncation pattern, resulting in a value called $\langle dE/dx \rangle_{trunc}$ which approximates a track's most probable dE/dx value.

dE/dx is a function of $\beta\gamma$, or p/m, as seen in Fig 9.[2] This means that heavy, slow-moving particles will have a high dE/dx. Most particles in the Standard Model are much lighter than the targeted chargino or stau masses, meaning that long-lived charginos or staus produced in the ATLAS detector will have a much higher $\langle dE/dx \rangle_{trunc}$ than Standard Model sources with high momentum, making it a powerful discriminant between the two.

The disappearing track signature is what occurs when a charged particle decays to soft and neutral secondardies within the detector. The neutral secondaries cannot be detected and the soft secondaries are not reconstructed as a part of the original track. As a result, the track appears to "disappear" in between

[2] $\beta = \frac{v}{c}$ and γ is the Lorentz factor, $\frac{1}{\sqrt{1-\beta^2}}$.

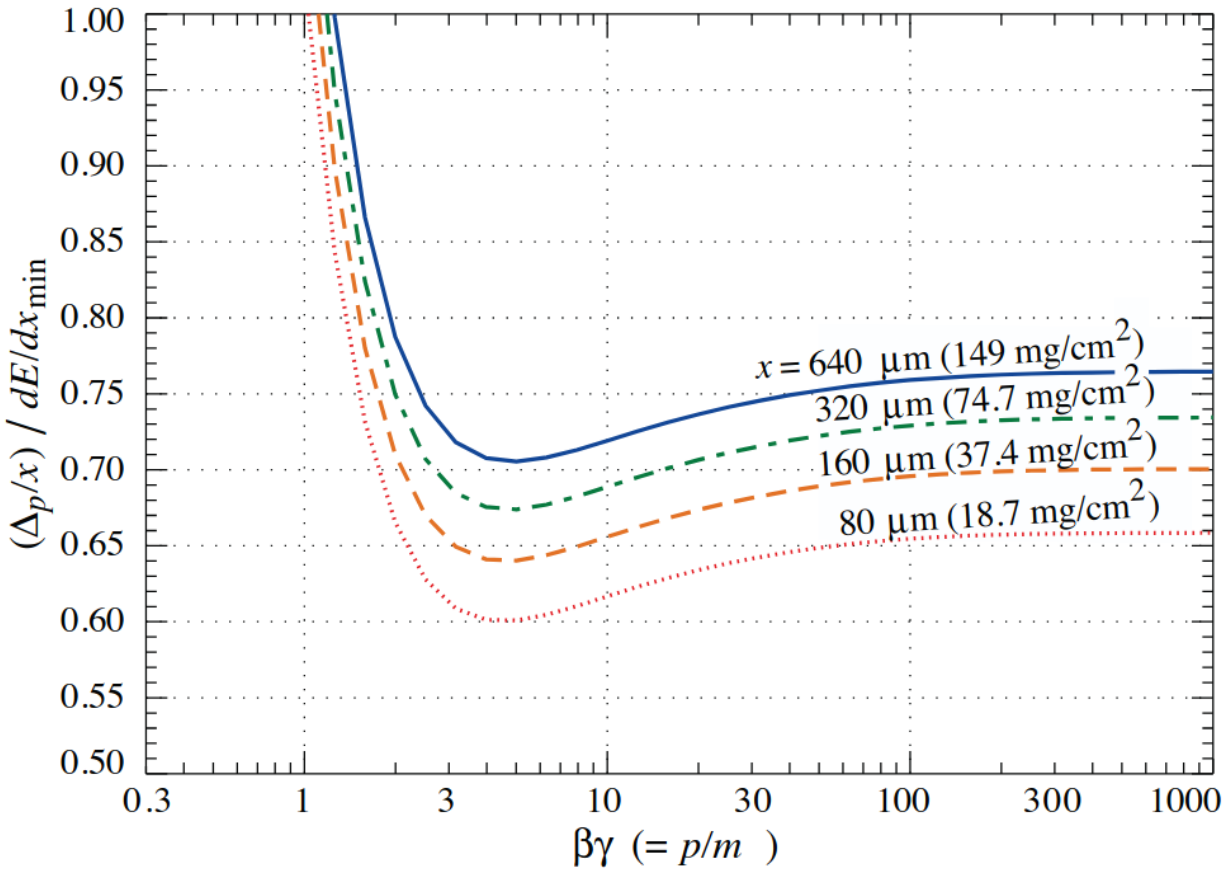

Figure 9: Bethe-Bloch curve for silicon [6].

the Pixel layers and SCT. This is a highly unique signature, and there are very few Standard Model sources that could duplicate it.

2.3.1 Backgrounds

The disappearing track search had two primary sources of background, the hadronic and leptonic background, and a fakes based background, examples of which are shown in Fig 10. The hadronic and leptonic backgrounds arise from a charged particle passing through the pixel layers and then scattering off some material or magnetic field in between the pixel detector and SCT. This causes a shift in direction for the particle, resulting in the rest of the track not being reconstructed as a part of the original object. These are called "kinked" tracklets, and, due to being both rare events as well as Standard Model sources, are expected to be heavily surpressed by the dE/dx requirement, as seen in Fig 11.

The other significant background that dominated the Run 2 disappearing track analysis came from combinatorial fakes. Tracks are reconstructed from collections of hits within the detector, with an algorithm grouping together hits that appear as thought they belong together. However, sometimes the algorithm groups hits that come from different sources. This causes the appearence of a fake track, a track that is composed of a number of hits from different sources rather than a single source. These events can have a high $\langle dE/dx \rangle_{trunc}$ due to individual high dE/dx hits contained within them. These types of events will be much more difficult to select against, making them the expected primary background of the analysis, and

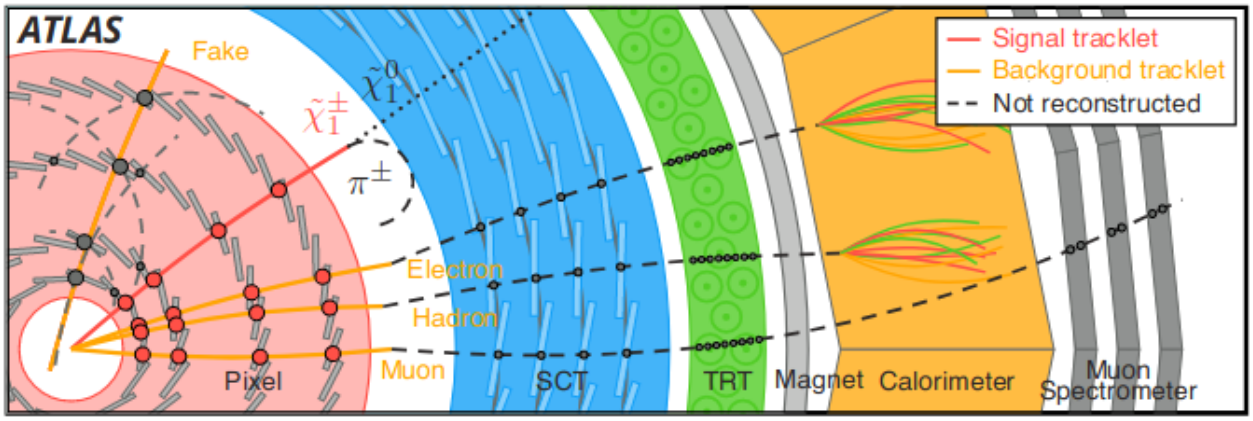

Figure 10: Signal and potential backgrounds within the ATLAS Detector [5].

motivating the need to study additional ways to discriminate against them.

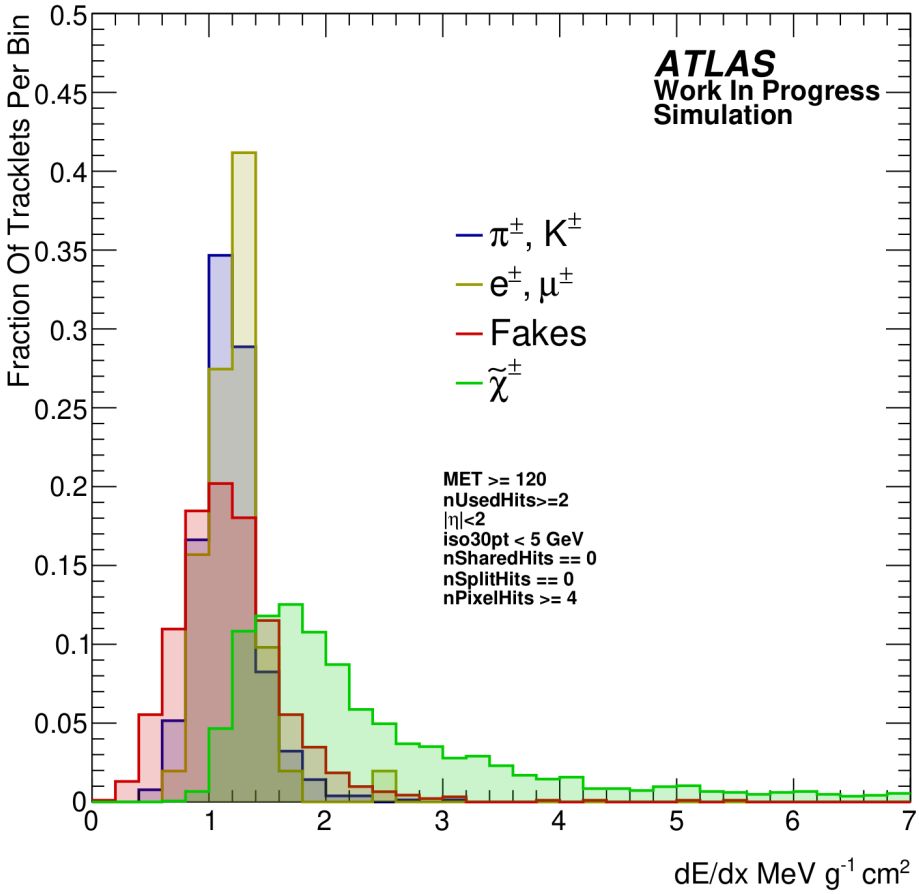

Figure 11: dE/dx_{trunc} distributions for signal and different potential sources of background.

2.4 Selections

We are attempting to remove as much background as possible while leaving as much signal as possible intact. To this end we use selections on the events present in the data. By understanding the effect that these selections have on both our signal and background, we can maximize the ratio between the two. The work of this thesis is focused on identifying additional selections that can be used to reduce the fakes-based background. There are some pre-selections that have been identified by the analysis team (informed from the Run 2 dE/dx and disappearing track-based searches) that ensure we are only selecting from high quality events and events that would be likely to contain signal. These include tracklets being required to have an $|\eta| > 2$ and 2 or more hits being used for calculation of $\langle dE/dx \rangle_{trunc}$ as well as a MET > 120 GeV. There are, additionally selections designed to ensure that only quality tracklets are being chosen. Tracklets must be sufficiently isiolated (iso30pt < 5 GeV) and have no shared or split hits.

2.5 ABCD Method

One way to estimate background is with an $ABCD$ method. If there are two variables that are uncorrelated, we can split the parameter space formed by them into four regions (named, as one might expect, A, B, C, and D). An example of these regions can be seen in Fig 12. By choosing values for these variables such that all signal events would fall within a single region (typically chosen to be region D), the number of background events in region D can then be esimated as;

$$\frac{N_A}{N_B} = \frac{N_C}{N_D}$$

$$N_D = \frac{N_B N_C}{N_A}$$

This estimation implicitly assumes that the ratio holds, which will only be true if the variables are sufficiently uncorrelated within the regions of interest.

This is one potential option to provide a background estimation for the dE/dx and disappearing track analysis provided we are able to identify two sufficiently uncorrelated variables.

2.6 Samples

In an effort to maintain blinding and not bias ourselves towards any particular result, analyses in ATLAS often use Monte Carlo simulations of data rather than the actual data recorded from our detector. With Monte Carlo samples, we can focus on specific processes, both in signal and background. Additionally, because we simulate these events, we can record what actually happened at the truth level. We can also use some data, so long as we are careful to remain blinded.

For this work, a variety of samples were used. An MC23E sample $Z^0 \to \mu^\pm\mu^\pm$ with full truth information was used as a general background. A version with cluster information was used for any studies focusing on using that information. Two signal samples were used, a $\tilde{\chi}^\pm$ MC23E sample was used as a general signal sample and a 800 GeV, 1 ns $\tilde{\tau}^\pm$ MC23E sample was used for cluster studies.

In addition, around $700,000$ $Z^0 \to \mu^\pm\mu^\pm$ events from ATLAS Run 3 data with cluster level information were used due to a sampling issue present in the MC23E file (see Section 2.6.1). These events have been

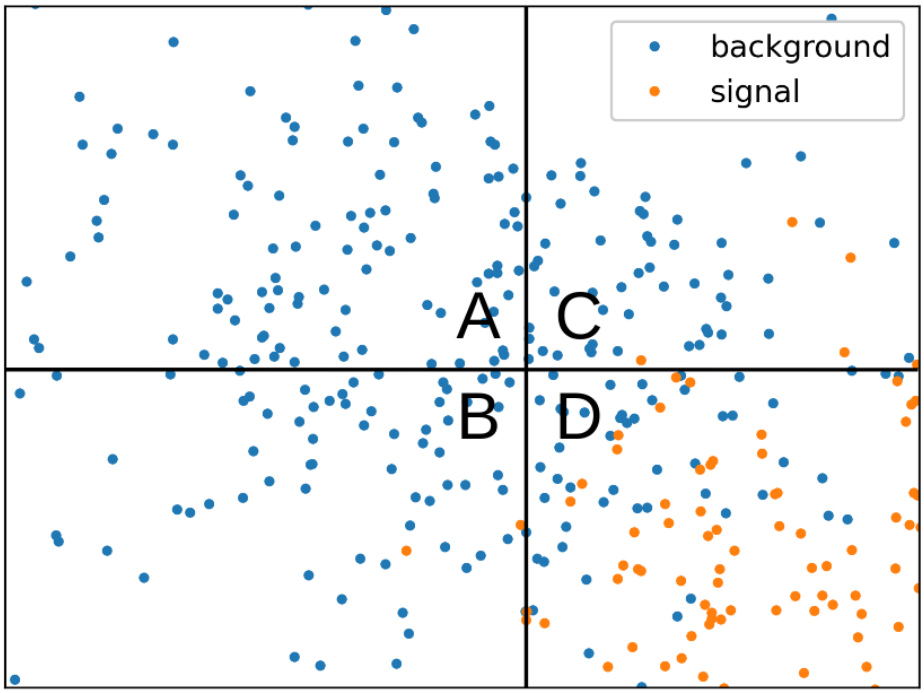

Figure 12: An example setup for an ABCD method. Signal events live almost entirely in region D [4].

reconstructed as containing a $Z^0 \to \mu^{\pm}\mu^{\pm}$ process, and can be carefully used in place of a Monte Carlo sample for background studies.

2.6.1 Data-MC Validation

The Monte-Carlo simulated samples that contained cluster level information were unnable to be used due to a reconstruction error that became evident in the high dE/dx regime. As seen in Fig 13, it appears as though the small number of background events are highly concentrated around specific values, a behavior that we suspected was nonphysical. Further investigation revealed that each spike was populated with copies of the same event, and was the result of Monte-Carlo samples not fully simulating pile-up events. This meant that we could not draw accurate conclusions from plots made with these samples.

We decided to use data to study our background, but in order to do so with confidence, we needed to see how well our simulation agreed with data.

In Fig 14, the calculation of the track level dE/dx value is plotted for both simulated signal and background. They agree to a high level, indicating that our Monte Carlo is an accurate reflection of the data, and that we will be able to use our Run 3 data as a background sample.

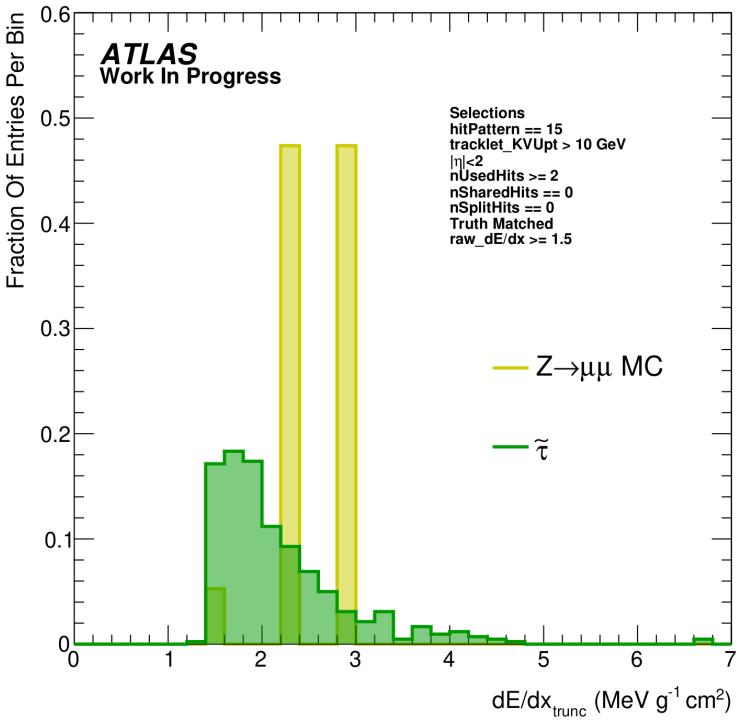

Figure 13: Track level dE/dx as calculated from clusters in simulated signal and background. The simulated background appears to have discrete spikes at certain values.

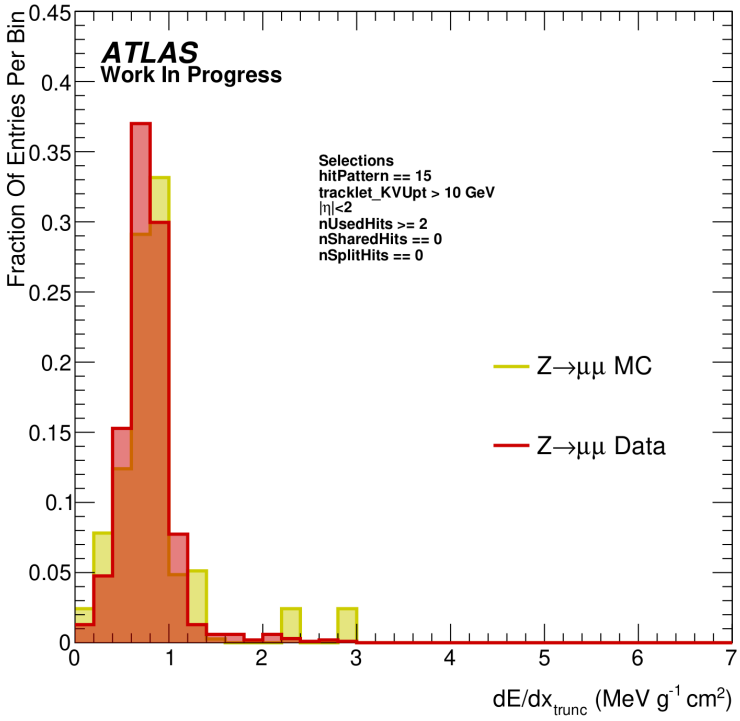

Figure 14: Calculated track-level dE/dx for both simulated background and Run 3 $Z^0 \to \mu^{\pm}\mu^{\pm}$ events.

3 Results

3.1 Tracklet Reconstruction Options

A potential method to suppress the fake background would be to implement a momentum cut of 10 GeV on all tracklets. This would, ideally, cut away a large portion of fakes, which we expect to be reconstructed with low momentum. The issue is that due to the short length scale of tracklets ($\mathcal{O}(10$ cm$)$) and the $1/L^2$ scaling of $\sigma(p_T)$, many fakes are reconstructed with a much higher momentum than they actually have, as seen in Fig 15. However, by applying a vertex constraint (assuming a tracklet originates from a primary vertex), we add additional length to our reconstructed objects ($\mathcal{O}(3$ cm$)$), and the measured p_T should be much closer to the actual value.

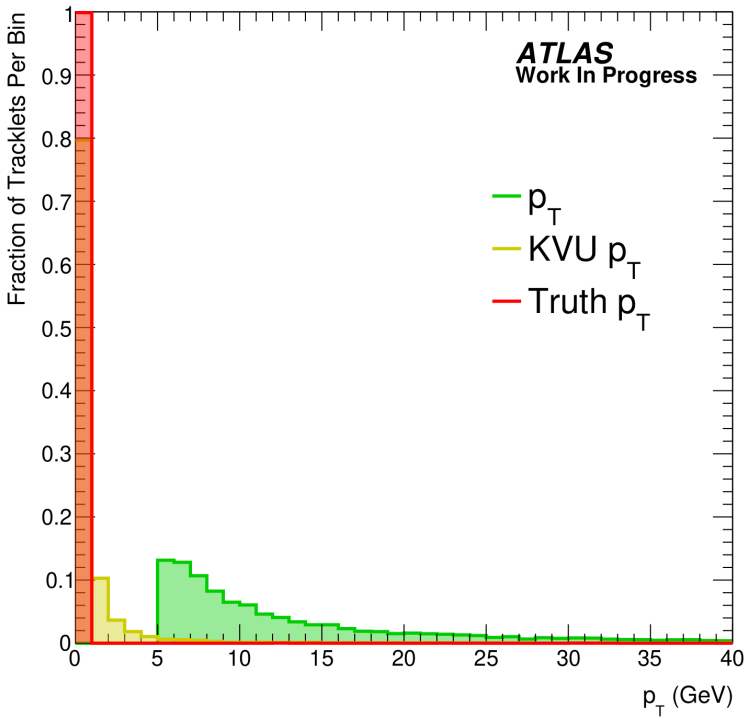

Figure 15: Reconstructed and KVU p_T distributions for our background.

We can see the efficiency of this selection in Fig 16. The application of the vertex constraint cuts away a large amount of background, with there being $\mathcal{O}(10$x$)$ fewer surviving tracklets. In signal the vertex constraint being applied actually results in a small, but noticable, increase in yield. This result indicates that the combination of a $p_T > 10$ GeV cut in combination with a vertex constraint is a highly efficient method of reducing background.

3.2 ABCD Correlation Studies

In order to use the $ABCD$ method for the dE/dx and disappearing track analysis, sufficiently uncorrelated variables would need to be selected. In order to see how correlated two variables are, there are a couple of metrics to consider. From a two-dimensional histogram of our two chosen variables (shown in Fig 17) we can simply choose to plot the mean of one variable as a function of the other. Uncorrelated variables will have no change in the mean, and correlation would appear as a nonzero slope.

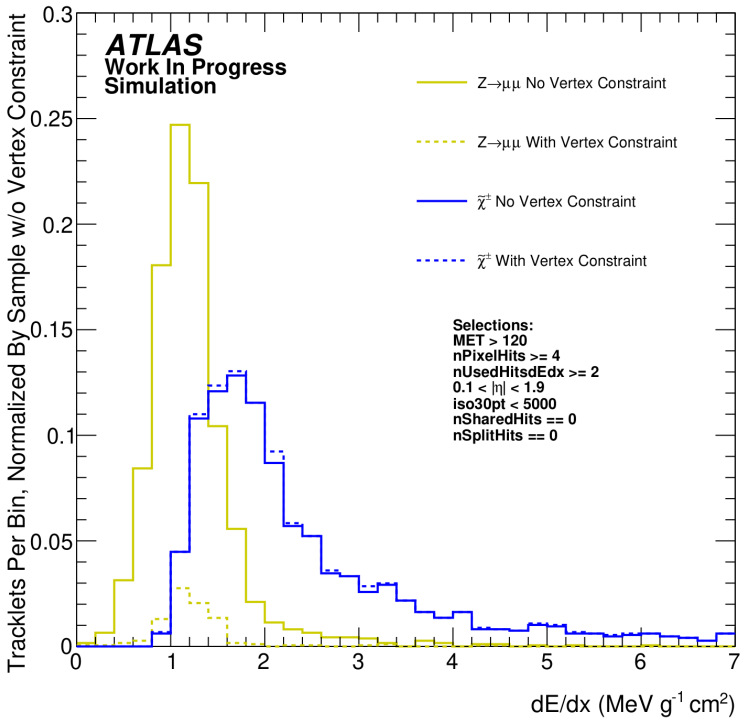

Figure 16: $\langle dE/dx \rangle_{trunc}$ distribution in simulated signal and background, both with and without a vertex constraint applied.

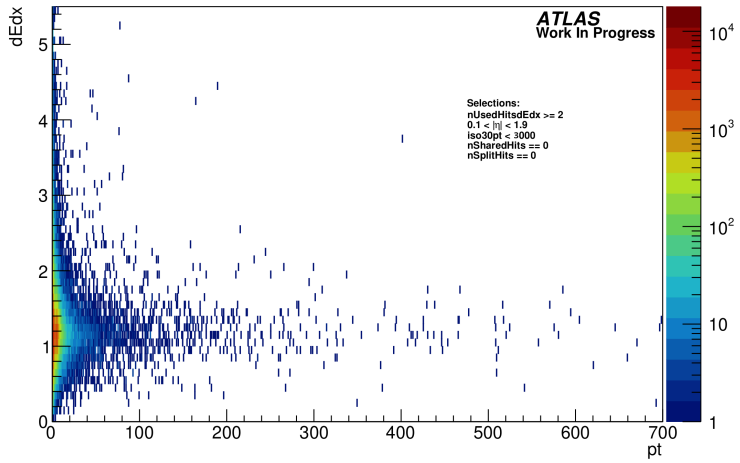

Figure 17: dE/dx vs. p_T in $Z^0 \to \mu^{\pm}\mu^{\pm}$ MC events.

Two natural choices for uncorrelated variables are dE/dx and p_T. The relation between the two is shown in Fig 17. The mean dE/dx as a function of p_T is shown in Fig 18. The mean is flat as a function of p_T, a good sign that the two lack correlation.

But this is not the only way in which two variables may be correlated, the mean dE/dx value might be consistent across many different p_T values, but its distribution may not be. We can measure this sort of correlation using a tail fraction as a metric. The tail fraction is the porportion of events that occur above a certain threshold value. If we select different p_T bands, we can see how the tail fraction changes as a function

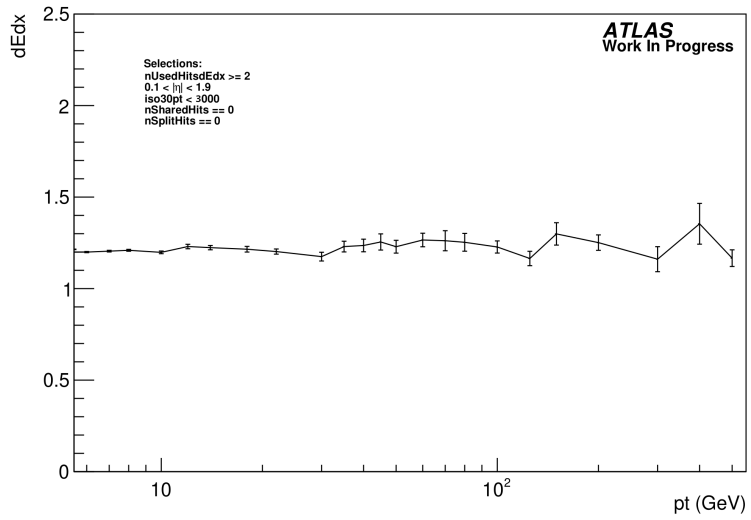

Figure 18: Mean dE/dx as a function of p_T in $Z^0 \to \mu^{\pm}\mu^{\pm}$ MC events.

of dE/dx. This is shown in Fig 19. There is a very obvious change in tail fraction behavior across various p_T values. This level of correlation suggests that dE/dx and p_T might not be ideal variables for an $ABCD$ method.

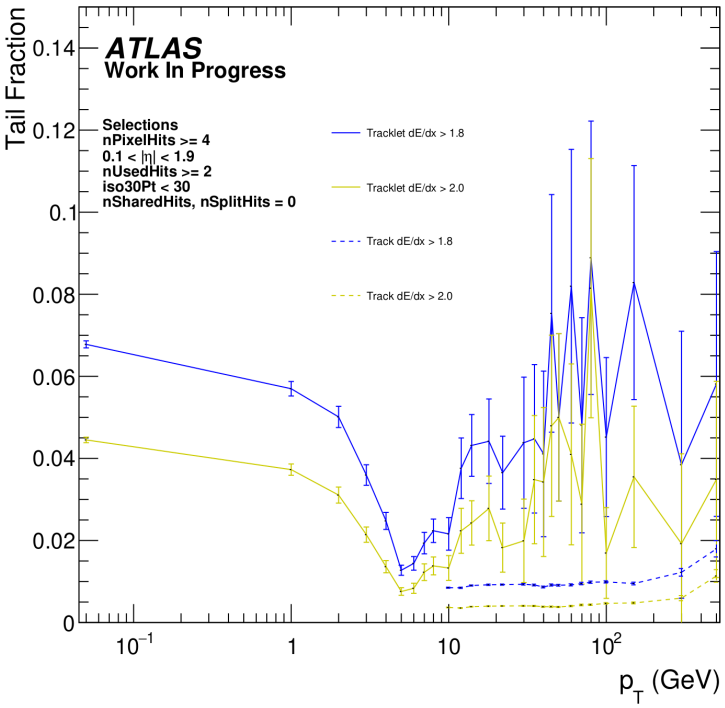

Figure 19: Tail fraction of dE/dx values as a function of p_T bands in $Z^0 \to \mu^{\pm}\mu^{\pm}$ events.

Another potential option was to see how dE/dx and z_0 were correlated. The tail fraction of this relationship however, displayed interesting behavior (Fig 20).

At low values of z_0, the tail fraction is consistent, but as tracklets originate from further away from

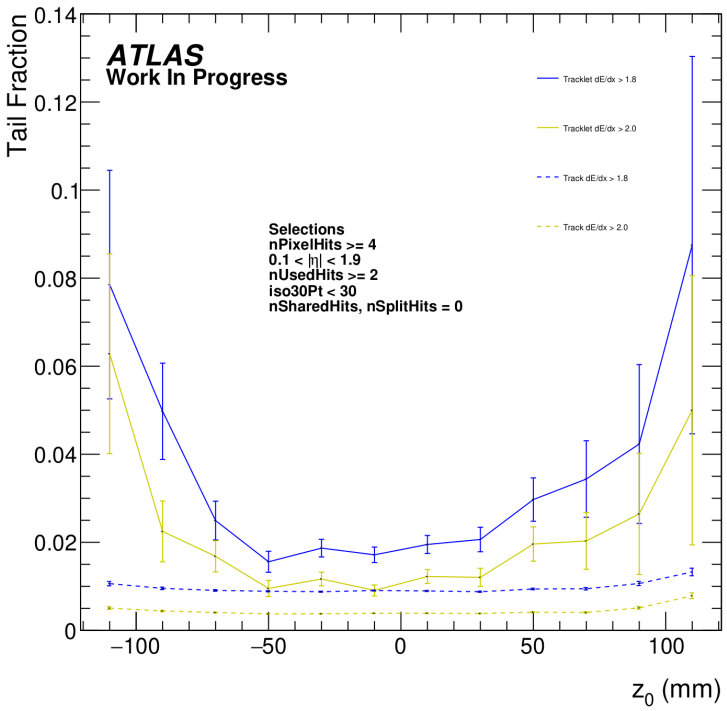

Figure 20: Tail fraction of dE/dx as a function of z_0 bands in $Z^0 \to \mu^\pm\mu^\pm$ events.

the beamline, their dE/dx distribution significantly widens. This behavior was unexpected and warranted further investigation.

3.3 Background Composition

One potenial option for the odd dE/dx, z_0 tail fraction behavior was that there were two separate backgrounds composing the near-beamspot and removed-from-beamspot regimes.

This motivated investigating the way the background was composed as a function of our impact parameters. Due to the MC23 samples having full truth information, the source of each tracklet that survived selection can be identified, allowing us to see exactly what source of background is dominant as a function of some chosen parameter.

There is a very clear increase in the amount of fake tracklets (defined by us as having a truth match < 0.5, meaning less than %50 of its hits are associated with a real track) as we become increasingly spatially removed from an event's primary vertex. This tells us that the background very close to the primary vertex is very different than the background that originates from other points further away from the primary vertex of an event.

3.4 Cluster Based Selections

A potential source of additional information that could be used as a method of discrimination is from the pixel clusters themselves. Much information is lost in the calculation of the final value of $\langle dE/dx \rangle_{trunc}$, and that information could potentially be useful. By using metrics derived from the additional information we

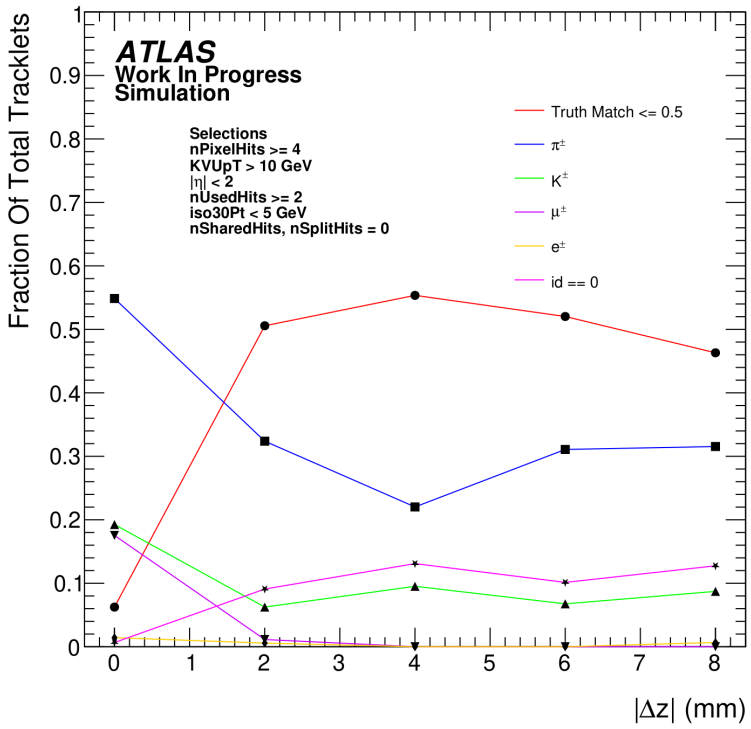

Figure 21: Background composition as a function of Δz.

gain, we can potentially find a selection to effectively discriminate against background that would otherwise have been unnavailable to us.

To identify a metric to use as a selection, the Z score[3] (significance) of each selection point was plotted for the high dE/dx regime to see whether a valuable cut could be made. This was studied for many metrics, including: The high dE/dx hit of the clusters that survive trncation, the average dE/dx of excluded clusters, the average dE/dx of the clusters *other* than the included high, the difference between the included high and average of the other values, the RMS of all cluster dE/dx values, and the layers that were dropped during truncation as well as the layer of the high dE/dx hit. Two metrics proved to be of particular interest.

The average of the other dE/dx values included in a tracklet asides from the highest hit (shown in Fig 22) showed a remarkable separation between signal and background, with a selection around a dE/dx value of $1-1.2$ being able to remove a significant portion of background while simultaneously not touching almost any signal events. This result indicates that many background events have a high dE/dx due to an additional high dE/dx hit that is not removed during truncation, with the rest of their hits having a much lower average dE/dx.

Additionally, the layers that are dropped during truncation (Fig 23) also showed a good ability to discriminate against background, with many of the highest dE/dx hits in background coming from the first two layers of the Pixel Detector, in particular the IBL. This behavior is unique to the high dE/dx regime, and without an additional tracklet level dE/dx selection, is largely hidden, as seen in Fig 24.

One potential explanation for this behavior is that the high dE/dx tracklets within our background gain their high dE/dx due to another real low-incidence angle particle grazing the inner detector and contributing the charge it deposits. This particle would contribute its charge loss entirely in that cluster without being

[3]Defined as $Z = \sqrt{2\left((s+b)\ln\left(1+s/b\right)-s\right)}$ [20].

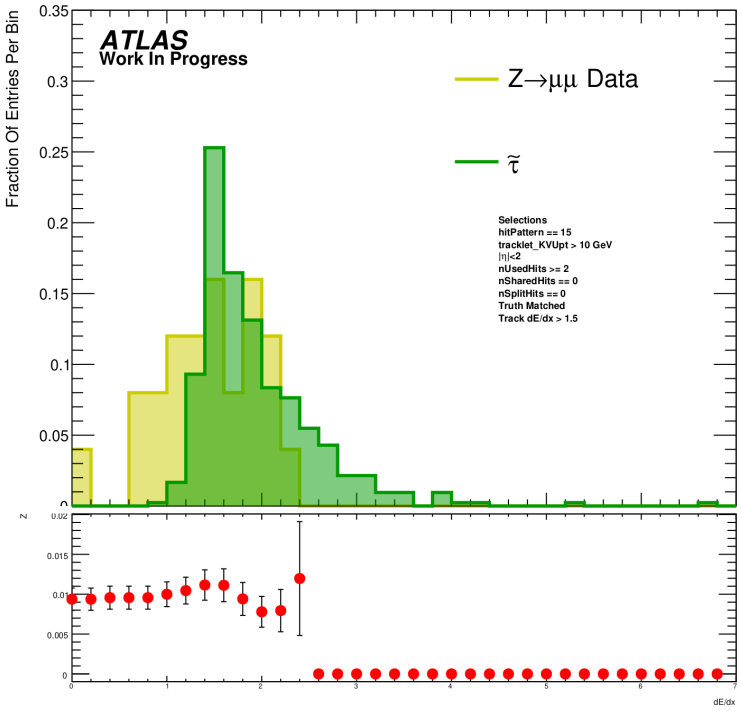

Figure 22: Average dE/dx value of tracklets excluding their highest hit that passes truncation. Also shown are the significance scores of potential cuts, with red dots representing selecting up and blue dots representing selecting down.

reconstructed later within the dector. This would make it appear as that cluster had an abnormally high dE/dx.

In order to test this hypothesis, we looked at the size of background tracklets in both η and ϕ. As seen in Fig 25 it is clear that, in background, the dropped clusters that come from the IBL are larger in size than those that come from layers further into the detector, whereas in Fig 26 we can signal the size is consistent throughout the pixel detector. This implies that there are different mechanisms causing high dE/dx hits for the innermost part of the pixel layers and the outermost layers and is consistent with the hypothesis that the high dE/dx cluster in background gets it high energy from a very shallow particle grazing the innermost layer and depositing charge.

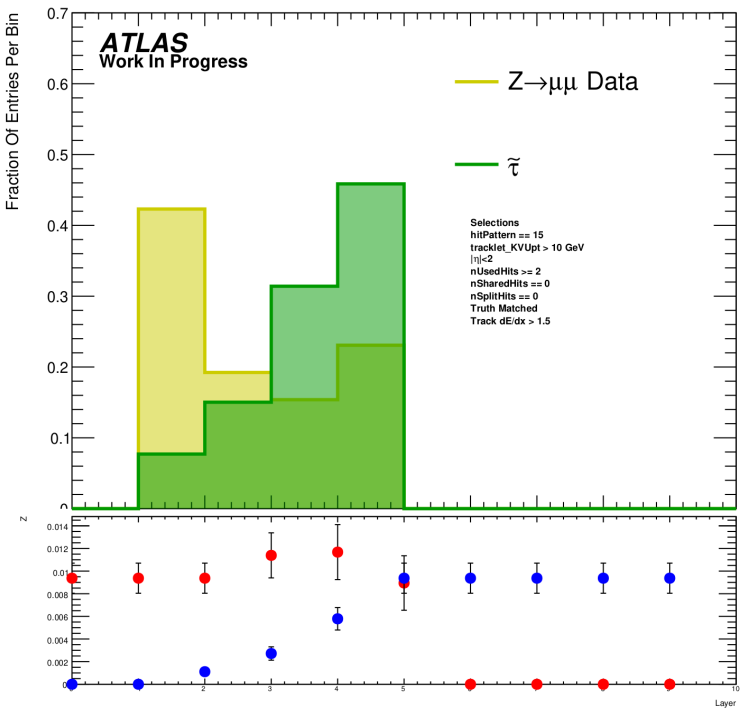

Figure 23: Which layer clusters that are dropped during truncation come from. Also shown are the significance scores of potential cuts, with red dots representing selecting up and blue dots representing selecting down.

4 Discussion

The ongoing dE/dx and disappearing track signature search is at the frontier of high energy searches for new physics, using unconventional detector signatures to further our understanding of the universe. This work focuses on the behavior of the potential backgrounds of this search, seeking a way to select against these backgrounds in favor of signal. These selections were targeted at a primarily combinatorial fake background, seeking to use the known properties of fake tracklets as a basis for selection.

The use of a vertex constraint to improve the efficacy of a 10 GeV cut on transverse momentum was based on the fact that, for a fakes based background, the distribution of normally reconstructed p_T would be much wider than p_T reconstructed with a vertex constraint due to improved momentum resolution. This additional requirement was highly effective at reducing background, and slightly improved signal yield.

To evaluate the potential for the analysis to use an $ABCD$ method to estimate its background, the correlation of several potential variables was studied. We could not confidently come to the conclusion that the variables we were interested in were uncorrelated.

These studies led to an investigation of the composition of our background as a function of our impact parameters. Because combinatorial fakes are not real particles, they do not need to come from a real interaction, and so their spatial origin was expected to be much more diffuse than any real source of background. This was confirmed, and we concluded that any background event coming from outside of the primary vertex was more likely to be a fake tracklet than a real particle.

Finally, we investigated the novel use of cluster level information to provide additional metrics to base a selection on. Many potential metrics were considered, with the most promising being a selection on the

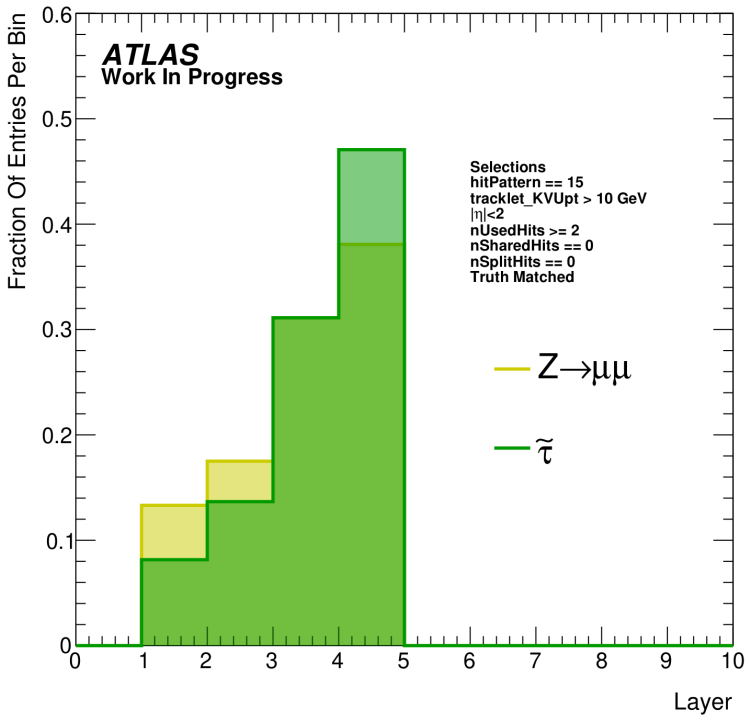

Figure 24: Which layer clusters that are dropped during truncation come from, without a tracklet level $1.5 > dE/dx$ selection.

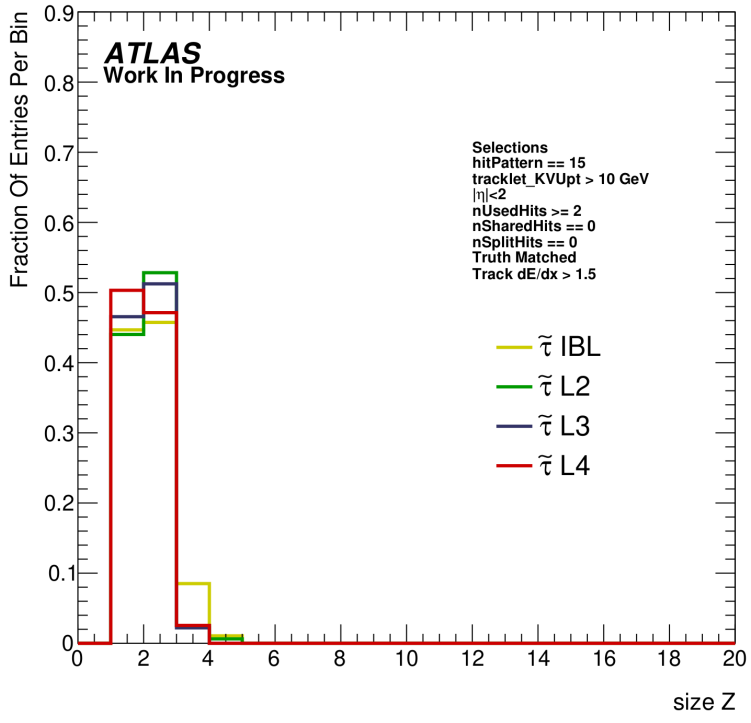

Figure 25: Number of pixels in dropped clusters in the η direction for simulated signal events.

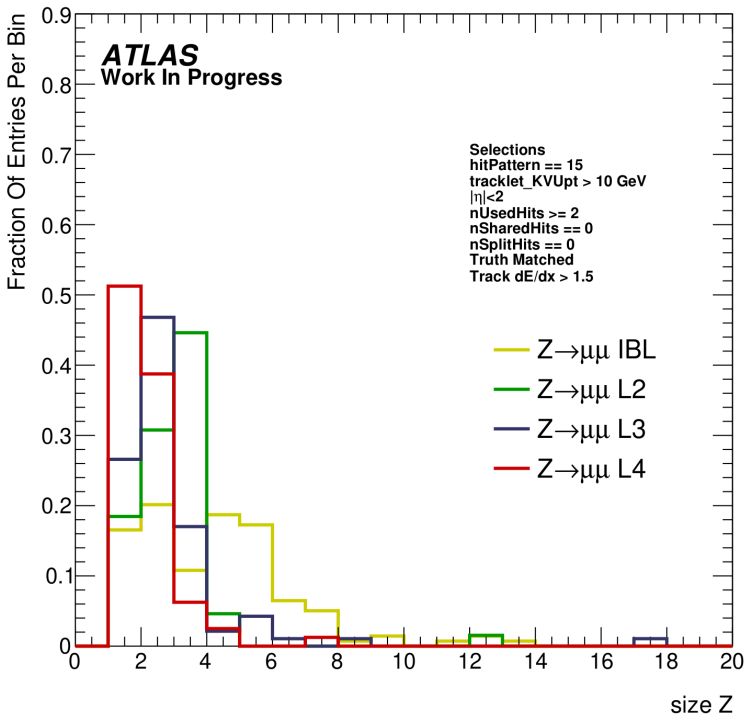

Figure 26: Number of pixels in dropped clusters in the η direction for background events.

average of the average of the cluster dE/dx values aside from the high included in the truncated mean, and a selection based off of which layer is dropped during truncation. We also were able to better understand how high dE/dx hits occur within the IBL, showing that clusters that have a high dE/dx value are spatially larger than high dE/dx clusters from further in the pixel layers.

5 Conclusions and Next Steps

This work has identified several key features of a predominant background for a combined disappearing track and dE/dx signature search. We have identified the use of a vertex constraint as optimal for minimizing background due to improved momentum resolution, studied the correlation between dE/dx and several other variables for a potential $ABCD$ method to estimate our background. We have shown that our background is predominantly composed of fake tracklets for tracklets that are spatially removed from the primary vertex. Finally we have identified a pair of potential metrics utilizing cluster-level information that could be used as the basis for a selection to discriminate against background events, as well as finding a potential way in which our background gains high dE/dx hits.

For the future of these studies, we will look to see if we can address the low significance values that the cluster based selections currently have by loosening existing selections as well as changing a signal model to more accurately reflect what we will have sensetivity to. We will also continue to investigate the source of high dE/dx clusters in background events.

References

[1] W. Yao *et al.*, "Review of particle physics," 2006.

[2] R. Carney, *Silicon Tracking and a Search for Long-lived Particles*. PhD thesis, Stockholm University.

[3] A. Collaboration, "The atlas experiment at the cern large hadron collider: A description of the detector configuration for run 3," 2023.

[4] A. Lory, *Search for new physics in signatures of soft unclustered energy patterns with the ATLAS detector*. PhD thesis, Ludwig Maximilian University of Munich, 2022.

[5] A. Collaboration, "Search for long-lived charginos based on a disappearing-track signature using 136 fb^{-1} of pp collisions at $\sqrt{s}$ = 13 TeV with the ATLAS detector," July 2022. arXiv:2201.02472 [hep-ex].

[6] S. Navas *et al.*, "Review of particle physics," *Phys. Rev. D*, vol. 110, no. 3, p. 030001, 2024.

[7] D. Griffiths, *Introduction To Elementary Particles*. Wiley-VCH, 2008.

[8] T. S. B. G. G. Fan, X. Myers, "Measurement of the electron magnetic moment," *Physical Review Letters*, 2023.

[9] H. Shao, J. J. Givans, J. Dunkley, M. Madhavacheril, F. Qu, G. Farren, and B. Sherwin, "Cosmological limits on the neutrino mass sum for beyond-λcdm models," 2024.

[10] B. Ryden, *Introduction to Cosmology, 2nd Edition*. Cambridge University Press, 2016.

[11] K. Strassler, M. Zurek, "Echoes of a hidden valley at hadron colliders," *Physics Letters B*, 2007.

[12] I. F. Ginzburg, M. Krawczyk, and P. Osland, "Two-higgs-doublet models with cp violation," 2002.

[13] H. Allanach, B. Haber, "Supersymmetry, part 1," 2024.

[14] J. Feng, "The wimp paradigm: Theme and variations," *SciPost Phys. Lect. Notes*, 2022.

[15] L. Lee, C. Ohm, A. Soffer, and T.-T. Yu, "Collider Searches for Long-Lived Particles Beyond the Standard Model," *Progress in Particle and Nuclear Physics*, vol. 106, pp. 210–255, May 2019. arXiv:1810.12602 [hep-ex, physics:hep-ph].

[16] M. D. Schwartz, "TASI Lectures on Collider Physics," Sept. 2017. arXiv:1709.04533 [hep-ph].

[17] T. A. Collaboration, "Observation of a new particle in the search for the standard model higgs boson with the atlas detector at the lhc," *Physics Letters B*, 2012.

[18] A. Collaboration, "Search for heavy, long-lived, charged particles with large ionisation energy loss in pp collisions at $\sqrt{s} = 13~\text{TeV}$ using the ATLAS experiment and the full Run 2 dataset," May 2022. arXiv:2205.06013 [hep-ex].

[19] C. Collaboration, "Search for supersymmetry in final states with disappearing tracks in proton-proton collisions at 13 tev," 2023.

[20] A. Collaboration, "Formulae for estimating significance," 2020.